International Journal of Advanced Research in Engineering and Technology (IJARET)
Volume 11, Issue 6, June 2020, pp. 59-79, Article ID: IJARET_11_06_007
Available online athttp://www.iaeme.com/IJARET/issues.asp?JType=IJARET&VType=11&IType=6
ISSN Print: 0976-6480 and ISSN Online: 0976-6499
DOI: 10.34218/IJARET.11.6.2020.007

LOWER BOUND LIMIT ANALYSIS OF PARABOLIC DOMES BASED ON SPHERICAL ANALYTICAL SOLUTION

R. Zona, L. Esposito, P. Ferla, S. Palladino, E. Totaro, V. Minutolo*
Engineering Department, University of Campania "L.Vanvitelli",
Via Roma 29 - 81031, Aversa (CE), Italy
*Corresponding Author E mail: vincenzo.minutolo@unicampania.it

ABSTRACT

The limit analysis of masonry structures is a topic of great interest and relevance, as these structures constitute a large part of the world's historical and cultural heritage. The authors proposed a formulation that allows evaluating the stability of curved structures like arches, vaults, and domes made of masonry and the calculation of the collapse multiplier of the applied loads. The approach has started from the analytical solution of the equilibrium of domes of revolution, obtaining the self-equilibrated stress by interpolating polynomials. Moreover, we calculated the actual elastic response of the structure by the finite element method. Finally, the used strategy superimposed the elastic stress to the self-equilibrated ones as the starting point of the optimization process. The procedure constitutes an effective way of assessing the structural safety and the limit load of structures; such an approach fulfills the requirements of the 'upper bound' theorem of the limit design. The proposed method can give a twofold response, namely the limit multiplier of prescribed load conditions and the safety assessment of a prescribed load level. The paper presented some examples of parabolical domes subjected to self-weight and variable loads; by applying the procedure, we calculated the load limits and the corresponding residual stress. Moreover, the thrust line at the incoming collapse is also derived.

Key words: limit analysis, lower bound, finite element method, parabolic domes, masonry, mixed finite element, no tensile resistant material

Cite this Article: R. Zona, L. Esposito, P. Ferla, S. Palladino, E. Totaro, V. Minutolo, Lower Bound Limit Analysis of Parabolic Domes Based on Spherical Analytical Solution, *International Journal of Advanced Research in Engineering and Technology*, 11(6), 2020, pp. 59-79.
http://www.iaeme.com/IJARET/issues.asp?JType=IJARET&VType=11&IType=6

1. INTRODUCTION

Structural analysis of ancient historic buildings is a delicate matter for engineers because used materials have many different behaviors that cannot be modeled in a standard way, due to anisotropy, heterogeneity, inelastic stress-strain law, and fragile rupture. Besides those constitutive characteristics, complex 3D geometry often characterizes the shape of ancient buildings that require detailed investigation to extract the actual structural model to input into the analysis process that is often, therefore, accompanied by significant indeterminacy. The stress and strain actual evaluation in structures is almost impossible since the loads vary randomly in time, as well as the boundary displacements due to subsidence. For these considerations and despite the complexity of the problem, the theory of plasticity, namely the limit analysis, can be a useful tool for the evaluation of the safety factor of structures and is widely used to assess the safety level of ancient and historical structures.

The primary necessity in the limit analysis context is, therefore, to define the limit domain where to search for stress that does not cause the collapse in the structure.

In this context, a first contribution is given by Heyman with the definition of a no – tensile stress domain for masonry [1]. Masonry as a no-tensile resistant material has been the subject of numerous studies also in the experimental field for the definition of a model that can predict its behavior until collapse [2, 3, 4] or the evaluation of the structural performance of masonry [5] and the consequently choice of the best material to build or re-build structures due to numerical or experimental evaluations [6, 7, 8, 9, 10].

The plasticity theory [11] provides a very powerful theoretical framework for the analysis of the limit state of structures when the static theorem is used in the context of equilibrium-based methods or kinematic theorem [12] when one wants to evaluate the collapse mechanisms. This tool provides safe and effective alternatives to elastic analysis during the early stages of structural design and for the limit analysis of statically indeterminate existing structures [13, 14, 15]. Furthermore, it defines the level of structural safety in a rather direct way through the collapse load factor (collapse multiplier). The limit analysis is a common approach when it is needed to study the stability of masonry structures such as arch bridges and masonry vaults [16]. Very interesting and useful methods, as well as accurate, have been developed in the last decades in this sense.

The main procedures used by practitioners consists of applying the kinematical Greenberg-Prager theorem to calculate an upper bound of the collapse load factor [17]. The individuation of collapse mechanisms is the basis of the kinematical approach applicability. The procedure consists of finding the minimum load factor among that in equilibrium on any kinematically admissible mechanism.

From the kinematic analysis point of view, the contribution is made by the formulations by finite elements [18] on the stability of vaults and domes [19], and in nonlinear problems [20, 21].

Recent studies propose the application of limit design by implementing the thrust line analysis (TNA). The thrust line is the locus of the points where the stress resultant acting on the cross-section of the structure is applied [22, 23, 24].

A first attempt to apply the thrust line method is the work of Méry (1840) [25], who developed the theory from the principle that the collapse of masonry arches occurs when there is such a sufficient amount of cracks along the arc to transform it into a mechanism. These cracks reduce the cross-section of the arc to behave like a hinge. The hinge develops whether no equilibrated stress is possible that does not violate the compatibility condition. Under the ordinary hypotheses, the compatibility consists that no tensile stress arises. No tensile stress occurs when the truss line remains within a prescribed region of the structure's cross-section.

This formulation is made assuming three fundamental hypotheses: infinite compressive strength, zero tensile strength, and no rupture due to sliding. The recalled hypotheses allow us to describe the masonry material as a rigid perfectly plastic material.

In Mery's proposed approach, the thrust line is the funicular curve of the applied loads. Recently, [8] and [9] extend the method to vaults and domes, respectively. In the three dimensional cases, the thrust line has changed into a thrust network yielding to a Thrust Network Analysis (TNA) [22, 26].

An evolution of the TNA approach has been presented with the Constrained Thrust Network Approach (CTNA), where the TNA is considered together with the geometrical constraint of the thrust locus [27, 28].

These works widen the concept of thrust line (or the curve of the pressures), creating a network of curves that represents a discretization of a thrust surface. Such a network allows widening the problem to the 3D domes. [29]

The phenomenological approach, as described above, can be considered to belong to the static limit analysis. The static equilibrated stress is described through the envelope line of the resultant of the stress, i.e., the thrust line. The compatibility constraint is the belonging of the thrust line to an admissible portion of the cross-section. In this sense, the static approach represents an alternative way to the kinematic approach.

Through lower bound analysis many studies have been performed to evaluate the stability of slope [30], in combination with Control Volume Finite Element [31], with variational concepts [32], due to linear programming [15, 5] or nonlinear programming [33] or second-order cone programming [34, 35].

The present work has proposed a numerical method that is based on the superimposition of self-equilibrated stress to the actual elastic stress solution for revolutionary domes. The method investigated the optimal self-equilibrated stress that allowed to fulfill the compatibility constraints of the material in terms of thrust surface. The self-equilibrium is solved using the homogeneous form of the equilibrium equation for domes. The so obtained self-stress has been discretized using polynomial interpolation. Finally, two different optimization programs have been considered: the first is to find the minimum of objective function consisting of the distance of the thrust line to the middle plane of the dome under the compatibility constraints and prescribed load level; the second is to find the maximum of the load multiplier.

The two proposed programs could be considered: the first, as the safety assessment under prescribed load level; the second, as a collapse multiplier of applied loads finding tool. Both approaches have been presented through several examples of domes. The results have been compared with Finite Element Analysis using ANSYS commercial code.

In the next section, the limit analysis methods are briefly recalled, and the application to no tensile resistant materials is specified. In the next section, the discretized procedure has been exemplified and particularized to domes of revolution. An ad hoc description of parabolical domes is proposed allowing for analytically to solve the equilibrium equations. Moreover, the case study is solved through FEM program Ansys to get the elastic stress to be introduced into Melan's theorem optimization problem.

Finally, some examples have been reported describing the effectiveness of the method and comparison have been reported with respect to FEM collapse analysis. The equivalence of the method with the thrust method has also been discussed.

2. LIMIT ANALYSIS OF MASONRY VAULTS AND DOMES

For the sake of completeness in the following, a brief recall of the effective statements of the limit analysis has been reported. The lower bound theorem of limit analysis is hereafter briefly described, for complete discussion one can refer to (Lubliner):

Let the structure be subjected to a load program consisting of a set of volume and boundary forces $f^n$and p^n, $n \in \{1,2,\dots m\}$, a function of time. The time represents a parameter of the incremental process purely, but no dynamical effects arise on the structure. Moreover, the load intensities belong to a limited domain; hence it is possible to express the loads' variability employing a common multiplier k. The structure is made of elastic plastic standard material. Namely, the stress-strain constitutive equation links the reversible strain to the stress provided the stress belongs to the interior of the admissibility domain, K, and relates the permanent strain rate to the stress when the latter attain the domain boundary. As usual, we assumed that the strain energy in the elastic range and plastic dissipation rate at the yield limit were positive.

$$\sigma = \frac{\partial w}{\partial \varepsilon}, \sigma \in \overset{\circ}{\mathrm{K}} \dot{\varepsilon}^p = \dot{\lambda}\frac{\partial \pi}{\partial \sigma}, \{\sigma, \sigma + d\sigma\} \in \partial \mathrm{K} \qquad \frac{\partial w}{\partial \varepsilon} d\varepsilon \geq 0, \frac{\partial \pi}{\partial \sigma} d\sigma \geq 0 \tag{1}$$

The procedure to calculate the limit load multiplier has been based on the lower bound theorem in the form of Melan's theorem for time-variable load history. The time-independent limit load results as a particular case of the Melan's theorem. The statement of the theorem is:

Let $\bar{\sigma}$ be any self-equilibrated time-independent stress, called eigenstress. Moreover, let $\sigma^*(t)$ be the time-dependent elastic stress in the structure obtained from equilibrium with the actual load. Finally, $\dot{\varepsilon}^p$, is the permanent strain derivative occurring into the structure during the load path.

It results:

$$\lim_{t\to\infty} \dot{\varepsilon}^p = 0 \Leftrightarrow \exists \bar{\sigma}: (\sigma^*(t) + \bar{\sigma}) \in K, \forall t \tag{2}$$

It must be recalled that the vanishing limit of permanent strain rate is equivalent to neither collapse nor ratcheting occurs. In the following sections, the domain, the eigenstress, and the Melan's theorem formulation have been specialized to the masonry domes.

2.1. Compatibility Domain

The materials, the masonry structure was made by, are described as rigid plastic with the compatibility domain consisting of pure compressive stress (Heymann). At first, let us focus our attention on a one-dimensional structure constituting an arc. This being the first curved structure where the proposed method can be applied to clarify the procedure.

The arc is formed by a plane figure moving along the line of the arc. The figure centroid, say the arc cross section's centroid, moves along the arc curve. The cross-section of the arc is a rectangle whose dimensions are: h its height and b its width. The structure is subjected to a distributed load. The internal stress, acting on the cross-section of the arc, has the resultant and the resultant moment about the centroid of the section, say N and M, respectively. Such generalized stress can be reduced uniquely to a force, N, applied at a point of the cross-section, C. The point is defined as the center of thrust. The line of centers of the thrust of any cross-section is called the thrust line of the arc. Now, if the center of thrust lays within the core of the cross-section of the arc, the stress acting on any point of the cross-section is purely compressive hence belongs to the admissibility domain K.

In this case, the compatibility conditions constituting the limit domain for the masonry material, in term of axial stress resultant and moment, is represented by the following inequalities:

$$\begin{cases} \frac{N}{bh} - \frac{6M}{bh^2} < 0 \\ \frac{N}{bh} + \frac{6M}{bh^2} < 0 \end{cases} \Leftrightarrow \begin{cases} hN - 6M < 0 \\ hN + 6M < 0 \\ 0 < N \end{cases} \quad (3)$$

One can relax the condition (3) by considering that the stress can become null in a portion of the cross-section. This happens whether the thrust line lays into the arc thickness:

$$\frac{\boldsymbol{h}}{\boldsymbol{2}} < \frac{\boldsymbol{M}}{\boldsymbol{N}} < \frac{\boldsymbol{h}}{\boldsymbol{2}} \quad (4)$$

The position (4) allows rewriting the compatibility inequalities in (3) the following way:

$$\begin{cases} hN - 2M < 0 \\ hN + 2M < 0 \\ 0 < N \end{cases} \quad (5)$$

The limit domain can be modified if the tensile strength is assumed to be non-null finite, $\sigma_y^t \neq 0$ so that limit tensile axial force can be calculated by:

$$N_0 = \sigma_y^t hb \quad (6)$$

to be introduced in (3) and (5) yielding to:

$$\begin{cases} hN - 2M < N_0 h \\ hN + 2M < N_0 h \\ N < N_0 \end{cases}; \begin{cases} hN - 6M < N_0 h \\ hN + 6M < N_0 h \\ N < N_0 \end{cases} \quad (7)$$

The compatibility domain can be represented in the N, M plane as reported in Figure 1.

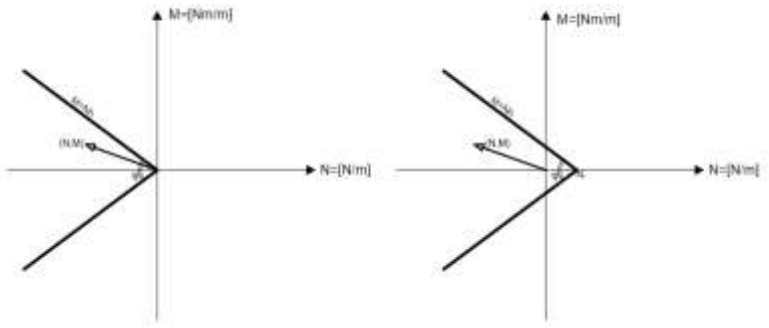

Figure 1 Compatibility Domain

2.2. Self-Equilibrated Solutions for Domes of Revolution

The equilibrium equation for a dome of revolution and the eigenstress domain have been described in the present section. The domain is obtained as the solution of the homogeneous form of the differential equation reported in Timoshenko [6]. The theory is briefly recalled in the following.

The equilibrium equations are written regarding a small element of surface, belonging to the middle plane of the dome, described by four section lines (Figure 2). Sections a-b and c-d are obtained along two meridian curves, and curves a-c and b-d are along two parallels, both at an infinitesimal distance.

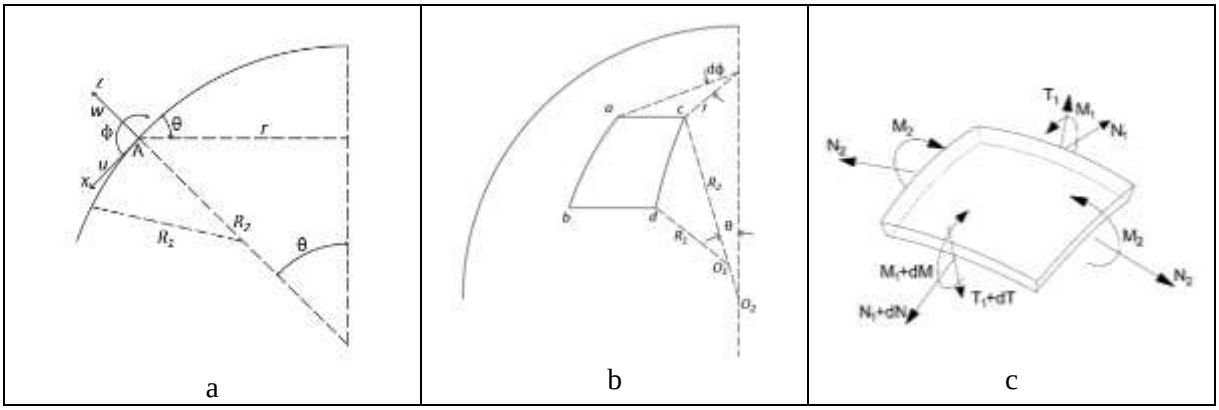

Figure 2 Geometric parameters (a), an infinitesimal element of the dome (b), and generalized stress on an infinitesimal element (c)

Regarding the Figure 2, the forces N_i, T_i and M_i are the generalized stresses per unit length, namely axial stress, shear and bending moment acting on the meridian curves for $i = 1$, and on the parallel for $i = 2$ respectively. Due to the dome symmetry, under the hypothesis that the loads have the same cylindrical symmetry of the structure, the stress and the displacement are independent on the longitude ϕ and are functions of the pure colatitudes θ. The balance of forces along the meridian, x direction, the outward normal, z direction, and the balance of the moments about the direction tangent to the parallel [6] yield to the equilibrium equations written in terms of the aforementioned generalized stress.

$$\begin{aligned} &\frac{d(N_1 r)}{d\theta} - N_2 R_1\, cos\theta - T_1 r = -X\, R_1 r \\ &N_1 r + N_2 R_1\, sin\theta + \frac{d(T_1 r)}{d\theta} = Z\, R_1 r \\ &\frac{d(M_1 r)}{d\theta} - M_2 R_1\, cos\theta - T_1\, R_1 r = 0 \end{aligned} \tag{8}$$

The equations (8) constitute a system of Ordinary Differential Equations ODE, and one can solve them by superimposing a particular solution to the general integral of its associated homogeneous form Equation (8).

From the mechanical standpoint, the homogeneous solution has the meaning of any time independent residual stress state that satisfies the equilibrium under vanishing load. In this perspective, the homogeneous solution assumes the meaning of eigenstress, and consequently, it is the equilibrium solution multiplicity as well.

The self-equilibrated solution is obtained simply by canceling the X and R component of external loads in equations (9).

$$\begin{aligned} &\frac{d(N_1^0 r)}{d\theta} - N_1^0 R_1\, cos\theta - T_1^0 r = 0 \\ &N_1^0 r + N_1^0 R_1\, sin\theta + \frac{d(T_1^0 r)}{d\theta} = 0 \\ &\frac{d(M_1^0 r)}{d\theta} - M_2^0 R_1\, cos\theta - T_1^0\, R_1 r = 0 \end{aligned} \tag{9}$$

2.2.1. Numerical Discretization

The numerical approximation of the solution of equation (9) is pursued using a set of shape functions. They belonged to the set of polynomials of degree n, depending on the colatitudes angle θ:

$$S_n(\theta) = \left[\theta^0, \theta^1, \ldots, \frac{\theta^n}{n!}\right] \qquad (10)$$

Five nodal parameter sets that multiply the shape functions (10) approximated the unknown self-equilibrated stresses, yielding to iso-parametric representation for all the stress functions.

$$\begin{cases} N_1 = \left[n_{1_0}, n_{1_1}, \ldots, n_{1_i}\right]^T \\ N_2 = \left[n_{2_0}, n_{2_1}, \ldots, n_{2_i}\right]^T \\ M_1 = \left[m_{1_0}, m_{1_1}, \ldots, m_{1_i}\right]^T \\ M_2 = \left[m_{2_0}, m_{2_1}, \ldots, m_{2_i}\right]^T \\ T_1 = \left[t_{1_0}, t_{1_1}, \ldots, t_{1_i}\right]^T \end{cases} \qquad (11)$$

Using coefficients (11), and shape functions (10) , the self-equilibrated stresses have been described by the following matrix form:

$$\begin{cases} N_1^0(\theta) = S_n(\theta) \cdot N_1 \\ N_2^0(\theta) = S_n(\theta) \cdot N_2 \\ M_1^0(\theta) = S_n(\theta) \cdot M_1 \\ M_2^0(\theta) = S_n(\theta) \cdot M_2 \\ T_1^0(\theta) = S_n(\theta) \cdot T_1 \end{cases} \qquad (12)$$

The derivatives of stress functions were

$$\begin{cases} \frac{dN_1^0(\theta)}{d\theta} = dS_n(\theta) \cdot N_1 \\ \frac{dN_2^0(\theta)}{d\theta} = dS_n(\theta) \cdot N_2 \\ \frac{dM_1^0(\theta)}{d\theta} = dS_n(\theta) \cdot M_1 \\ \frac{dM_2^0(\theta)}{d\theta} = dS_n(\theta) \cdot M_2 \\ \frac{dT_1^0(\theta)}{d\theta} = dS_n(\theta) \cdot T_1 \end{cases} \qquad (13)$$

where $dS_n(\theta)$ is the matrix of the derivative of the shape functions:

$$\mathrm{dS_n}(\theta) = [0, 1, \theta, \ldots, \theta^{n-1}] = [0] \cup \mathrm{S_{n-1}}(\theta) \qquad (14)$$

The differential equations (8) in discretized form have become:

$$\begin{aligned} &\left(\frac{dr}{d\theta} S_n(\theta) + r dS_n(\theta)\right) N_1 - S_n(\theta) R_1 \cos\theta \, N_2 - r S_n(\theta) T_1 = 0 \\ &S_n(\theta) r N_1 + S_n(\theta) R_1 \sin\theta \, N_2 + \left(\frac{dr}{d\theta} S_n(\theta) + r dS_n(\theta)\right) T_1 = 0 \\ &\left(\frac{dr}{d\theta} S_n(\theta) + r dS_n(\theta)\right) M_1 - S_n(\theta) R_1 \cos\theta \, M_2 - r R_1 S_n(\theta) T_1 = 0 \end{aligned} \qquad (15)$$

Finally, collecting all the parameters in a single vector $x = [N_1, N_2, M_1, M_2, T_1]$, self-equilibrium equations were rewritten in matrix form

$$Ax = 0 \qquad (16)$$

where the matrix A is a function of the angle θ, whose explicit expression is the following, where the dependence on θ was highlighted:

$$A(\theta)=\begin{bmatrix} \left(\frac{dr}{d\theta}S_n(\theta)+rdS_n(\theta)\right) & -S_n(\theta)R_1\cos\theta & 0 & 0 & -rS_n(\theta) \\ S_n(\theta)r & S_n(\theta)R_1\sin\theta & 0 & 0 & \left(\frac{dr}{d\theta}S_n(\theta)+rdS_n(\theta)\right) \\ 0 & 0 & \left(\frac{dr}{d\theta}S_n(\theta)+rdS_n(\theta)\right) & -S_n(\theta)R_1\cos\theta & -rR_1S_n(\theta) \end{bmatrix} \quad (17)$$

The equation (16) does not have a unique solution. However, one can find three of the unknown variables as a function of the remaining $5n-3$.

The matrix A is partitioned into a non-singular square matrix B, of rank 3, and a remainder part C of dimension $(3\times 5n-3)$ by reordering its columns. The vector x changes into a reordered form depending on A. Namely x divides into a part, b, of dimension 3, and a complementary part c. The first, b, contained the variables corresponding to the columns in B, and the second, c, contained the remainder ordered like C.

The equilibrium equation in discrete form is, hence, modified into the following:

$$[B \quad C]\begin{bmatrix} b \\ c \end{bmatrix}=0 \quad (18)$$

Or in the explicit form:

$$Bb+Cc=0 \quad (19)$$

By solving for b, one has:

$$b=Kc \quad (20)$$

where

$$K=-B^{-1}C \quad (21)$$

Within the manifold of discrete parameters x, the solution of the Equation (20) is the set of all the self-equilibrated stresses.

In conclusion, splitting Equation (20) into its parts related to stress components as reported in the Equation(11), one obtained the expression of stress parameters in terms of equilibrated ones.

$$\begin{aligned} N_1 &= K_{N1}c \\ N_2 &= K_{N2}c \\ M_1 &= K_{M1}c \\ M_2 &= K_{M2}c \\ T_1 &= K_{T1}c \end{aligned} \quad (22)$$

Equations (22) substituted into the equation (12) gives the discrete form of the eigenstress in the structure as a function of the equilibrated parameter set c.

2.3. Elastic Solution

Melan's theorem requires the knowledge of elastic stress produced by the applied load pattern. The elastic solution of the dome equilibrium must be pursued numerically except that for simple load cases for which a closed-form solution exists. The elastic solution has been calculated through a commercial FE code Ansys© that calculated the stresses along meridians and parallel curves for several applied loads.

The FEM mesh contained eight-node shell elements. The output has consisted of the nominal stress resultants N_i^e, M_i^e, T_i^e that have to be amplified by the multiplier k.

2.4. Numerical Optimization Strategy

The limit multiplier of prescribed load paths, either monotonically increasing or randomly variable, is obtained by maximizing the load multiplier under the constraint that the sum of elastic response, plus any self-equilibrated time-independent stress solution of (14), as a function of c, belong to the admissible domain. Hence it results that the optimization program has the load multiplier as objective function and the parameters c as variables. The optimization constraints are the linear inequalities representing the limit domain in terms of c.

At first elastic solution is obtained employing FEM analysis. In the proposed application, only axial stress and bending influence the safety of the structure since shear effects are negligible due to its rather small thickness. The vectors N_i^e, M_i^e collected the effective generalized stress where $i \in \{1, 2\}$ referred to the meridians or parallel direction, respectively. Collocating the equations at discrete angles, i.e., at a finite number of θ_j with $j \in \{1, \dots\dots, m\}$, where m was the number of points along the meridian curve, one gets the solution numerically.

The discretized form of the Equation (22)

$$\begin{cases} \mathrm{N}_1^{\mathrm{j}} = \mathrm{K}_{\mathrm{N}_1}^{\mathrm{j}}\mathrm{c} \\ \mathrm{N}_2^{\mathrm{j}} = \mathrm{K}_{\mathrm{N}_2}^{\mathrm{j}}\mathrm{c} \\ \mathrm{M}_1^{\mathrm{j}} = \mathrm{K}_{\mathrm{M}_1}^{\mathrm{j}}\mathrm{c} \\ \mathrm{M}_2^{\mathrm{j}} = \mathrm{K}_{\mathrm{M}_2}^{\mathrm{j}}\mathrm{c} \\ \mathrm{T}_1^{\mathrm{j}} = \mathrm{K}_{\mathrm{T}_1}^{\mathrm{j}}\mathrm{c} \end{cases} \tag{23}$$

where the superscript $(\quad)^j$ referred to the discrete angles θ_j.

Finally, the optimization program, starting from equation (5) has the following discretized form where the stress components, N_i^r and M_i^r, must be calculated via (23)

$$\sup_{\mathbf{c}} \mathrm{k} \left| \mathrm{k} \in \mathbb{R}^+ : \begin{cases} \mathrm{h}(\mathrm{N}_\mathrm{i}^\mathrm{r} + \mathrm{kN}_\mathrm{i}^\mathrm{e}) + 2(\mathrm{M}_\mathrm{i}^\mathrm{r} + \mathrm{kM}_\mathrm{i}^\mathrm{e}) < \alpha \\ \mathrm{h}(\mathrm{N}_\mathrm{i}^\mathrm{r} + \mathrm{kN}_\mathrm{i}^\mathrm{e}) - 2(\mathrm{M}_\mathrm{i}^\mathrm{r} + \mathrm{kM}_\mathrm{i}^\mathrm{e}) < \alpha \\ (\mathrm{N}_\mathrm{i}^\mathrm{r} + \mathrm{kN}_\mathrm{i}^\mathrm{e}) < \beta \end{cases}^{\mathrm{j}} \right. \tag{24}$$

where

$$\begin{cases} 0 \\ N_0 h \end{cases}, \beta = \begin{cases} 0 \\ N_0 \end{cases} \tag{25}$$

depending on the presence of tensile resistance σ_0 such that axial limit stress is $N_0 = \sigma_0 h$ following the material constitutive properties equations (3), (5), and (7). Following the same reasoning, one can state a second optimization program based on the same constraint inequalities (24). The second optimization program evaluates the safety of a prescribed load multiplier. Namely, for a prescribed load factor k, it searched if there exist any self-equilibrated stresses, N_i^r and M_i^r, such that the constraint equations hold. In this latter case, the formulation yield to a constrained minimum program, the objective function being the norm, $\wp$, of the difference between the actual eccentricity $e_{ij} = \left(\frac{M_i}{N_i}\right)_j$ and the limit eccentricity $h/2$ that corresponds to the stresses that violate the equilibrium and compatibility conditions. The resulting formulation has consisted of:

$$\min_{c} \wp \left| \wp \in \mathbb{R}^{+}, \wp = \sqrt{\sum_{j=1,m}\left[\sum_{i=1,2}\left(\frac{M_i^r + kM_i^e}{N_i^r + kN_i^e} - \frac{h}{2}\right)^j\right]^2} : \begin{cases} h(N_i^r + kN_i^e) + 2(M_i^r + kM_i^e) < \alpha \\ h(N_i^r + kN_i^e) - 2(M_i^r + kM_i^e) < \alpha \\ (N_i^r + kN_i^e) < \beta \end{cases} \right|^j \quad (26)$$

2.4.1. Case study Parabolic Dome of Revolution

The method described in the previous section has been applied to a parabolic dome of revolution. The structure model is a parabolic surface obtained by rotating a parabola curve about a vertical axis. For structural shape numerical treatment, it has been chosen that an arc of circumference approximated the parabola, the criterium of the approximation is reported graphically in Figure 3. The geometry of the dome middle surface has been derived approximatively from Brunelleschi's dome of Santa Maria del Fiore in Florence. The circular approximation of the dome middle surface allowed using more straightforward analytical calculation, parametric description, and versatile. Since approximation, one can rewrite the equilibrium equations (8) in terms of the sphere and of the parallel radii. The latter radius can be calculated as a function of the colatitude angle only.

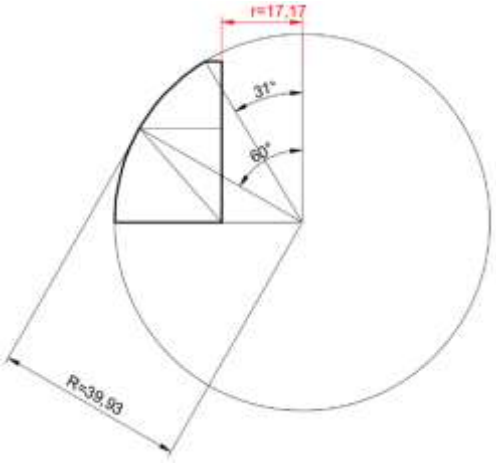

Figure 3 The approximation of parabolic geometry to circular geometry

2.5. Problem Formulation and Optimization Program

In the following, for simplicity, we have considered a structure with cylindrical symmetry. Hence, we analyzed only one meridian of the vault. The simplification of the geometry discussed in the previous section allowed using the equation of equilibrium for spherical shells.

We organized the load program of the analysis considering a first load step consisting of the self-weight of the structure that is supposed to be constant in time. A second load step has consisted of a ramped line load acting on a parallel of the dome. The evolutionary parameter k is the load intensity multiplier. Twofold load typology acted on the parallel, the first directed vertically and the second directed along the radial direction.

The formulation described the self-equilibrated stress in terms of the shape functions (10) and of coefficients (11). The elastic solution was the result of a FEM analysis using Ansys© commercial code.

The calculation has consisted of finding the collapse value of k, say sc, as the maximum k, for which the compatibility conditions hold. Furthermore, for several load multiplier less than collapse limit, we checked the safety of the structure as a confirm that the procedure is affordable.

The analytical part of the procedure involves the use of a routine written through the software Mathematica© [36].

The routine performed the twofold procedure, the first concerning the evaluation of the load collapse multiplier lower-bound by maximizing statically admissible stress, in the form of superimposition of the elastic response and self-equilibrated stress as described in the previous sections. The second procedure evaluated the safety of the structure under the prescribed applied load level indicated through the prescribed load multiplier k.

The numerical discretization of the method yielded to numerical approximation already quoted in the previous descriptions. The calculation previsedto discretize the meridian by dividing it into 20 segments, see Figure 4, where to collocate the compatibility inequalities and to calculate the elastic solution.

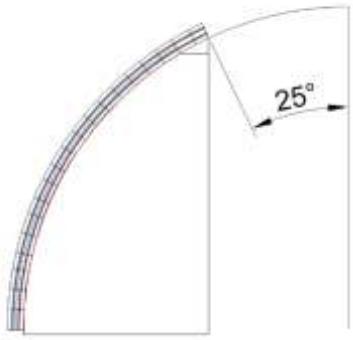

Figure 4 Discretized dome's meridian

Along with the load path application, the load multiplier results form the solution of the following optimization programs:

at first, the self-weight collapse multiplier resulted by solving:

Self-weight:

$$\sup_{(N^r,M^r)} k \left| \begin{cases} h(N_i^r + kN_i^e) - 2(M_i^r + kM_i^e) < \alpha \\ h(N_i^r + kN_i^e) - 2(M_i^r + kM_i^e) < \alpha \\ (N_i^r + kN_i^e) < \beta \end{cases} \right|_j \qquad (27)$$

In the equation (27), the vectors N_i^e and M_i^e contained only dead load stress results. As shown before, when other load conditions are applied, the safety factor k multiplies the vector of generalized stress induced by the variable loads only. The two analyzed load cases were solved using the mathematical programming synthesized in the equations reported hereafter.

Variable Loads:

$$\sup_{(N^r,M^r)} k \left| \begin{cases} h(N_i^r + N_i^e + kN_i^{VL}) + 2(M_i^r + M_i^e + kM_i^{VL}) < \alpha \\ h(N_i^r + N_i^e + kN_i^{VL}) - 2(M_i^r + M_i^e + kM_i^{VL}) < \alpha \\ (N_i^r + N_i^e + kN_i^{VL}) < \beta \end{cases} \right|_j \qquad (28)$$

Where $N_i^{VL}$and M_i^{VL} are the axial stresses and the bending moments due to variable loads.

2.6. Safety Assessment

The second approach refers to evaluating the safety of a prescribed load level. The load is affected by the known multiplier λ. The objective function depended on the design variables, namely (N_i^r, M_i^r)

$$\wp = \sqrt{\sum_{j=1,m}\left\{\sum_{i=1,2}[2(M_i^r + M_i^e + \lambda M_i^{VL}) - h(N_i^r + N_i^e + \lambda N_i^{VL})]_j\right\}^2} \qquad (29)$$

2.7. FEM elastic Solution

The FEM results have been obtained using ANSYS© commercial code. Figure 5 The model has been calculated using shell elements that map the middle surface of the dome and furnished, as an output, the generalized stress, namely axial forces and bending moments aligned along with the parallel and the meridian direction.

The geometric data input was:

Base diameter: 45.5 m.

Height = 34.75 m.

Thickness = 0.77 m.

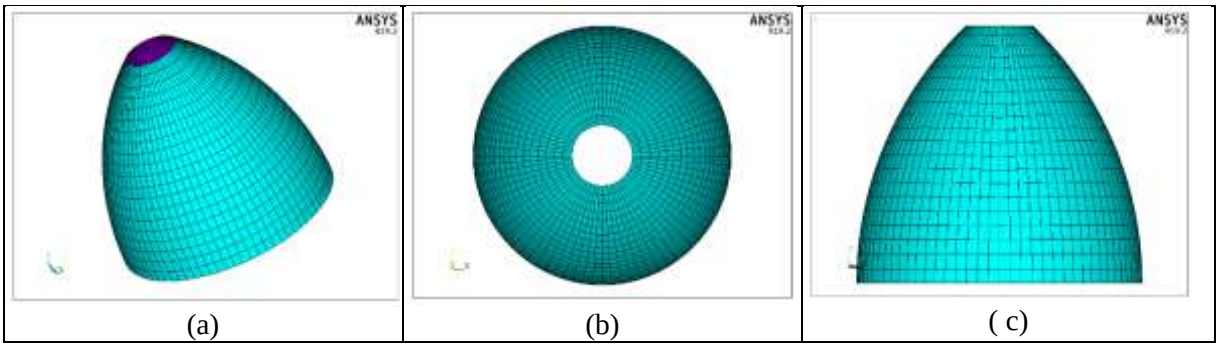

Figure 5 Dome model (a) 3D view; (b) Top view; (c) Front view.

The structure base circumference constraints assume fixed all the degrees of freedom; hence the base of the dome is clamped. Figure 6 represents the resulting reactions and nodal forces.

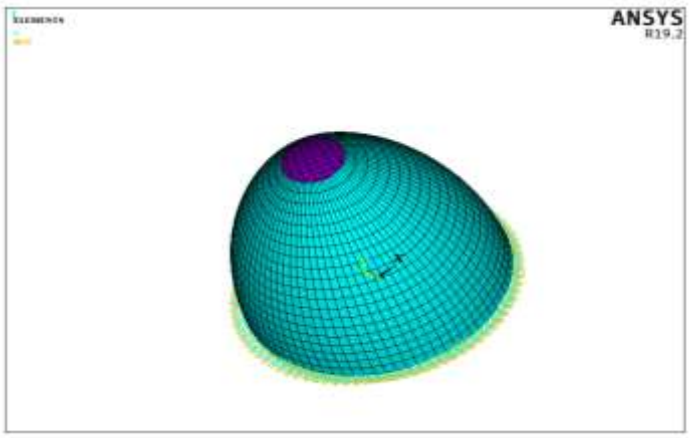

Figure 6 3D Dome with all boundary conditions.

Three load cases have been considered for the analysis:

- self-weight applied as density and uniform line load applied on the top parallel in the vertical direction that represents the top lantern to the dome, Figure 7
- uniform line load in radial outward (Figure 8), inward (Figure 9) and vertical (Figure 10) direction applied on a parallel corresponding to the angle $\theta_p, p\,\{5,10,15\}$. The Figures showed the case $p = 5$.

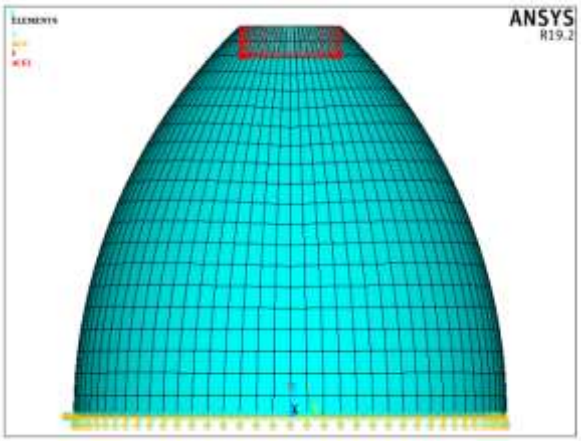

Figure 7 Load case: self-weight and lantern.

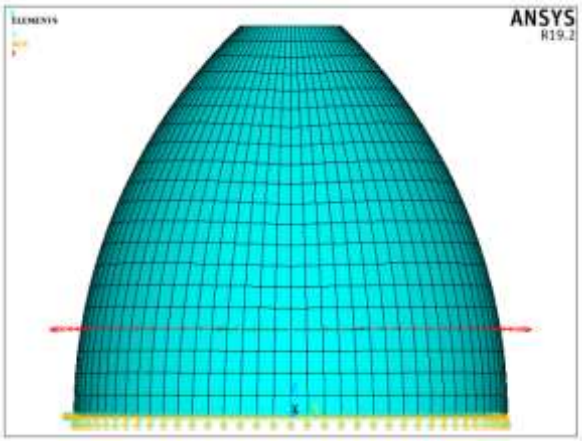

Figure 8 Load case: Radial outward load on 5th parallel.

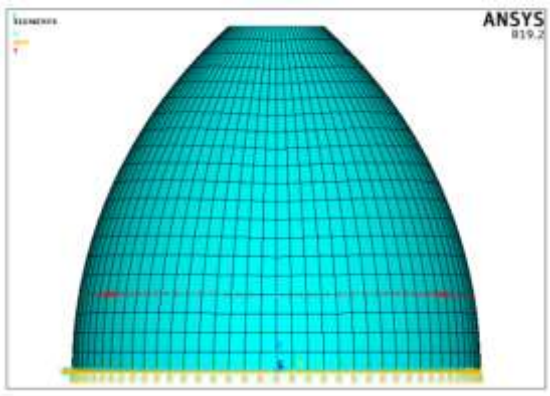

Figure 9 Load case: Radial inward load on 5th parallel.

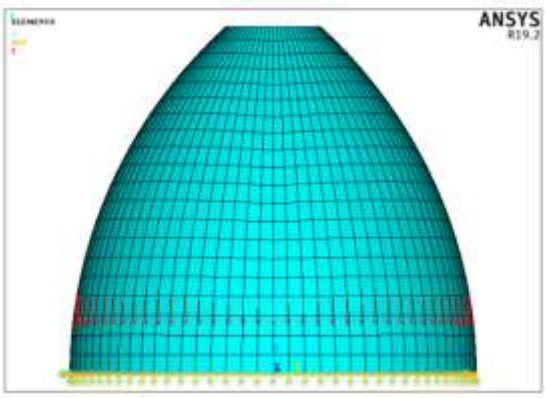

Figure 10 Load case: vertical directed load on 5th parallel.

In the Table 1, the mechanical properties of the structure are reported:

Table 1 Mechanical properties of the dome

Young modulus $\left[N/m^3\right]$	**Poisson's ratio**	**Weight** $\left[N/m^3\right]$
18000	0.27	18000

In the following Figure 11, the stress contour plots showed the distribution of the elastic response of the structure to the applied loads.

LOAD	**M_1**	**M_2**	**N_1**	**N_2**
Self-weight	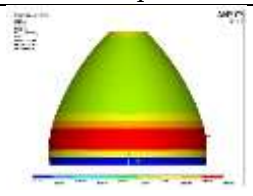	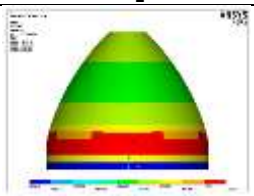	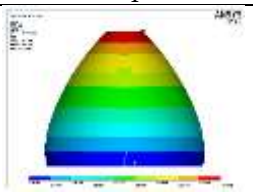	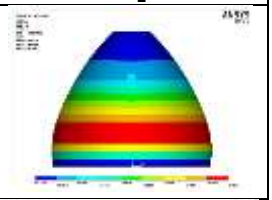
Radial outward load	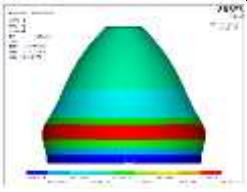	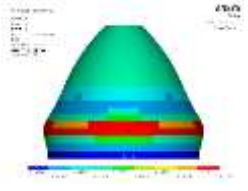	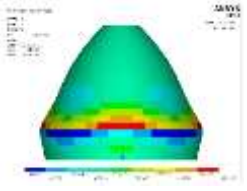	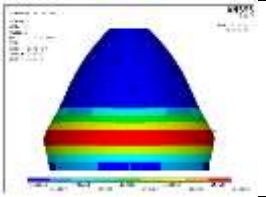

Radial inward load	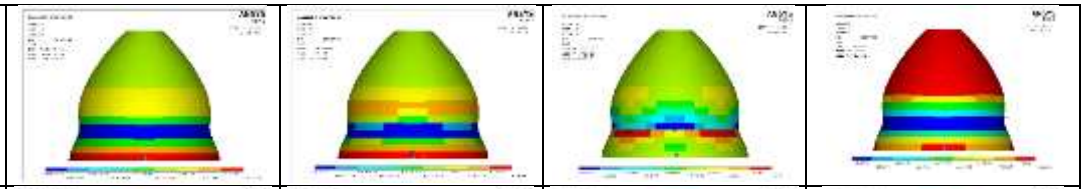			
Vertical load	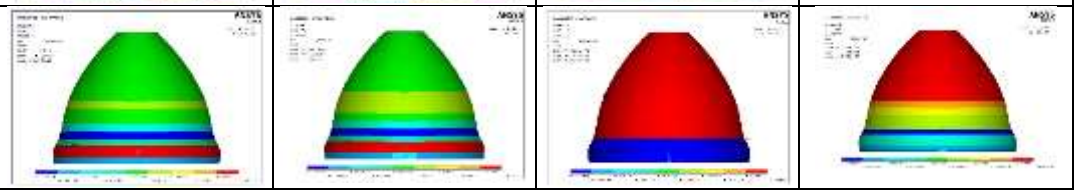			

Figure 11 Stress contour plot for different load condition

The following numerical arrays, Table 2, contained the results of the elastic calculation that one must introduce into the Mathematica© notebook that performed the optimization program:

Table 2 Numerical Value of stress vector corresponding to contour plot

Self-Weight + Lantern				
ELEM	**N_2**	**N_1**	**M_2**	**M_1**
1	-43.92	-196.21	-3433.9	-12777
21	-17.76	-183.71	286.91	768.93
41	9.329	-171.66	1717.7	6007.8
61	26.779	-160.33	1785.1	6438.5
81	33.036	-149.79	1245.1	4771.2
101	30.596	-139.98	581.92	2674.8
121	22.948	-130.78	34.249	950.56
141	13.077	-122.02	-326.7	-170.85
161	2.9757	-113.56	-520.15	-756.82
181	-6.2939	-105.32	-598.77	-981.26
201	-14.327	-97.2	-615.11	-1016
221	-21.082	-89.148	-606.82	-985.3
241	-26.653	-81.098	-593.69	-958.5
261	-31.13	-72.975	-580.39	-959.82
281	-34.526	-64.682	-560.34	-980.76
301	-36.792	-56.084	-519.1	-986.43
321	-37.862	-47.004	-436.42	-913.42
341	-37.949	-37.123	-296.94	-671.36
361	-38.033	-25.818	-121.32	-202.69
381	-41.557	-11.038	-63.902	69.371

Table 3 Numerical Value of stress vector corresponding to contour plot

Radial inward load				
ELEM	**N_2**	**N_1**	**M_2**	**M_1**
1	-1.67E-02	-3.51E-04	8.9586	33.705
21	-7.62E-02	-6.46E-04	4.6174	19.464
41	-1.73E-01	2.71E-04	-2.2304	-3.519
61	-2.63E-01	3.96E-03	-13.62	-45.173
81	-2.83E-01	-1.34E-02	-13.226	-46.807
101	-2.16E-01	-9.38E-03	-1.5643	-7.1739
121	-1.28E-01	-5.03E-03	3.6711	10.955
141	-5.60E-02	-1.64E-03	4.7509	15.223
161	-1.08E-02	3.61E-04	3.7778	12.615
181	1.08E-02	1.13E-03	2.2126	7.9067
201	1.64E-02	1.07E-03	0.8536	3.6765
221	1.38E-02	6.38E-04	-1.27E-02	0.86939
241	8.58E-03	1.56E-04	-0.40127	-0.52154
261	3.84E-03	-1.87E-04	-0.45841	-0.90856
281	7.43E-04	-3.36E-04	-0.34783	-0.76233
301	-7.04E-04	-3.23E-04	-0.19483	-0.44442
321	-1.01E-03	-2.16E-04	-7.06E-02	-0.16414
341	-7.48E-04	-8.63E-05	3.13E-04	-2.50E-03
361	-3.14E-04	1.39E-05	2.48E-02	4.15E-02
381	1.93E-04	3.17E-05	2.77E-02	1.98E-02

Table 4 Numerical Value of stress vector corresponding to contour plot

Radial outward load				
ELEM	**N_2**	**N_1**	**M_2**	**M_1**
1	1.67E-02	3.51E-04	-8.9586	-33.705
21	7.62E-02	6.46E-04	-4.6174	-19.464
41	1.73E-01	-2.71E-04	2.2304	3.519
61	2.63E-01	-3.96E-03	13.62	45.173
81	2.83E-01	1.34E-02	13.226	46.807
101	2.16E-01	9.38E-03	1.5643	7.1739
121	1.28E-01	5.03E-03	-3.6711	-10.955
141	5.60E-02	1.64E-03	-4.7509	-15.223
161	1.08E-02	-3.61E-04	-3.7778	-12.615
181	-1.08E-02	-1.13E-03	-2.2126	-7.9067
201	-1.64E-02	-1.07E-03	-0.8536	-3.6765
221	-1.38E-02	-6.38E-04	1.27E-02	-0.86939
241	-8.58E-03	-1.56E-04	0.40127	0.52154
261	-3.84E-03	1.87E-04	0.45841	0.90856
281	-7.43E-04	3.36E-04	0.34783	0.76233
301	7.04E-04	3.23E-04	0.19483	0.44442
321	1.01E-03	2.16E-04	7.06E-02	0.16414
341	7.48E-04	8.63E-05	-3.13E-04	2.50E-03
361	3.14E-04	-1.39E-05	-2.48E-02	-4.15E-02
381	-1.93E-04	-3.17E-05	-2.77E-02	-1.98E-02

Table 5 Numerical Value of stress vector corresponding to contour plot

Vertical Load				
ELEM	**N_2**	**N_1**	**M_2**	**M_1**
1	-3.08E-02	-0.12969	-0.98313	-3.6274
21	-2.46E-02	-0.1309	1.3564	5.125
41	-2.65E-02	-0.13237	1.4826	5.9605
61	-3.92E-02	-0.13399	-0.66183	-1.6481
81	-1.37E-02	2.90E-04	-1.7352	-5.8001
101	-1.49E-02	7.30E-05	-0.70372	-2.4001
121	-1.14E-02	1.20E-04	-8.28E-02	-0.33957
141	-6.78E-03	2.18E-04	0.19643	0.59603
161	-3.00E-03	3.00E-04	0.25379	0.80881
181	-6.21E-04	3.22E-04	0.20168	0.66339
201	5.00E-04	2.93E-04	0.11867	0.41135
221	7.89E-04	2.30E-04	4.74E-02	0.18791
241	6.49E-04	1.59E-04	2.73E-03	4.19E-02
261	3.80E-04	9.51E-05	-1.65E-02	-2.86E-02
281	1.41E-04	4.85E-05	-1.85E-02	-4.64E-02
301	-5.17E-06	2.00E-05	-1.24E-02	-3.73E-02
321	-6.54E-05	6.54E-06	-4.87E-03	-2.04E-02
341	-6.70E-05	2.48E-06	5.06E-04	-6.88E-03
361	-4.09E-05	2.97E-06	2.86E-03	-3.96E-04
381	-8.28E-07	2.04E-06	3.43E-03	5.28E-04

3. RESULTS AND DISCUSSION

The proposed procedure gave the limit multiplier and the residual stress at the incoming collapse resulting from the optimization program. The residuals represented the Melan's residuals that was not the actual ones but that arising from the program. The actual residuals depend on the load history and could be calculated only through step-by-step analysis. However, the self-stress (Figure 12) resulting from the program is one of the possible statically admissible stress. Figure 14 and 14 reported the thrust line obtained through the statically admissible stress along the structure abscissa.

The load pattern of self-weight does not produce the collapse of the structure, the load multiplier of such load program is unbounded, and the corresponding residuals were indeterminate. The meaning of such a result is that the load is unable to produce the collapse. We tested the same load pattern to assess the safety under some prescribed load multiplier and calculated the corresponding residuals by minimizing the eccentricity norm, Equation (28). As one expected, the second optimal program gave a finite solution, and the resulting residuals produced, summed with the elastic stress, vanishing eccentricity almost everywhere along the dome's axial curve.

Figure 14 represented the thrust lines with respect to the stress acting along the parallel; the curve has been drawn along with the meridian as well. in the figures of the latter example with the indication of the dome's thickness and the indication of the portion of the cross-section of the structure, located at the middle of the width, that represents the locus which the thrust line must belong to since the stress did not attain tensile value.

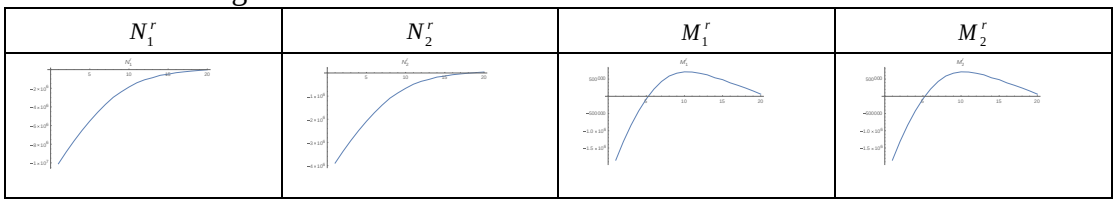

Figure 12 Typical residual stresses

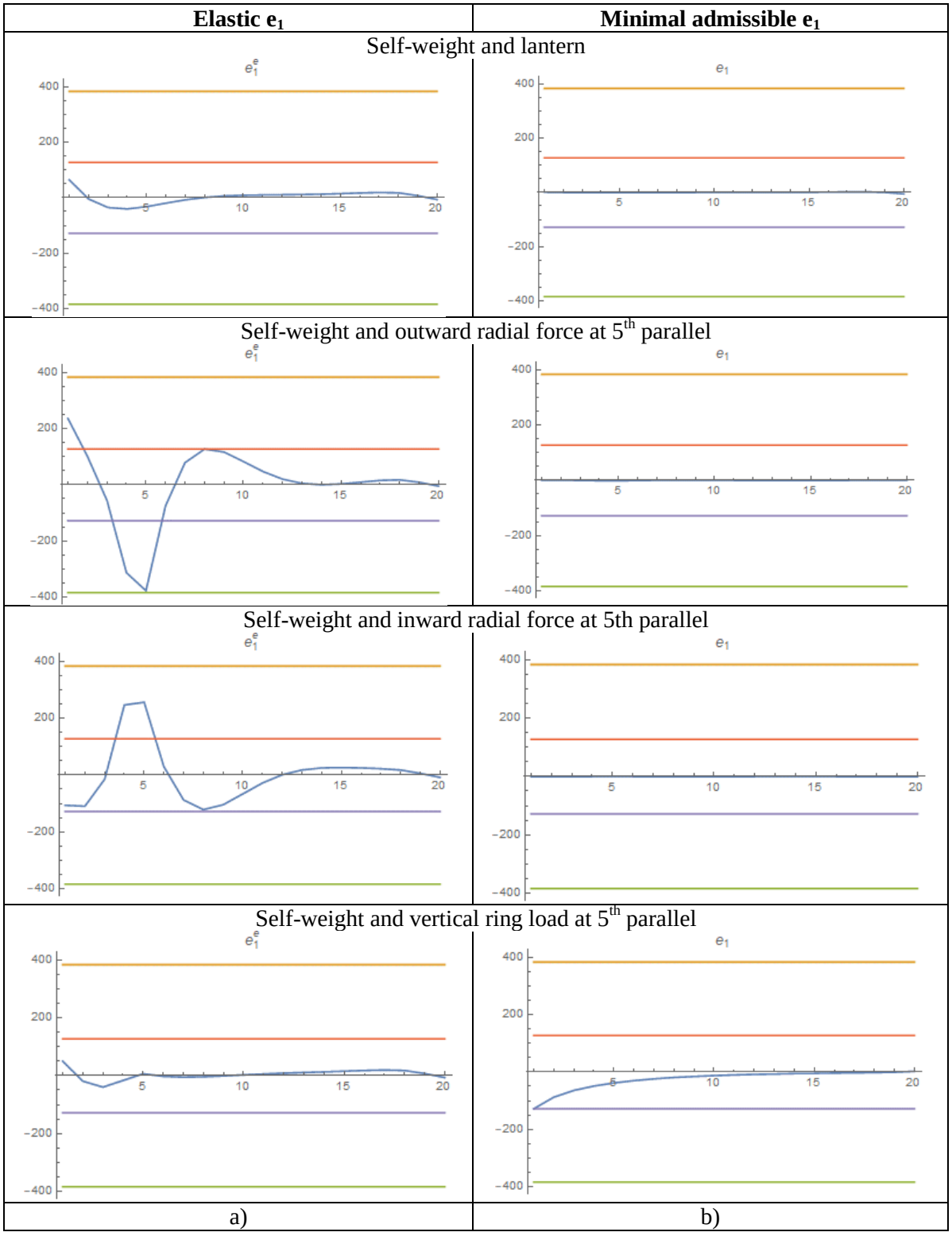

Figure 13 Trust line e_1 of the elastic solution along the meridian, solid lines represent thickness, green and orange cross-section limits lines, red and blue median third of the section

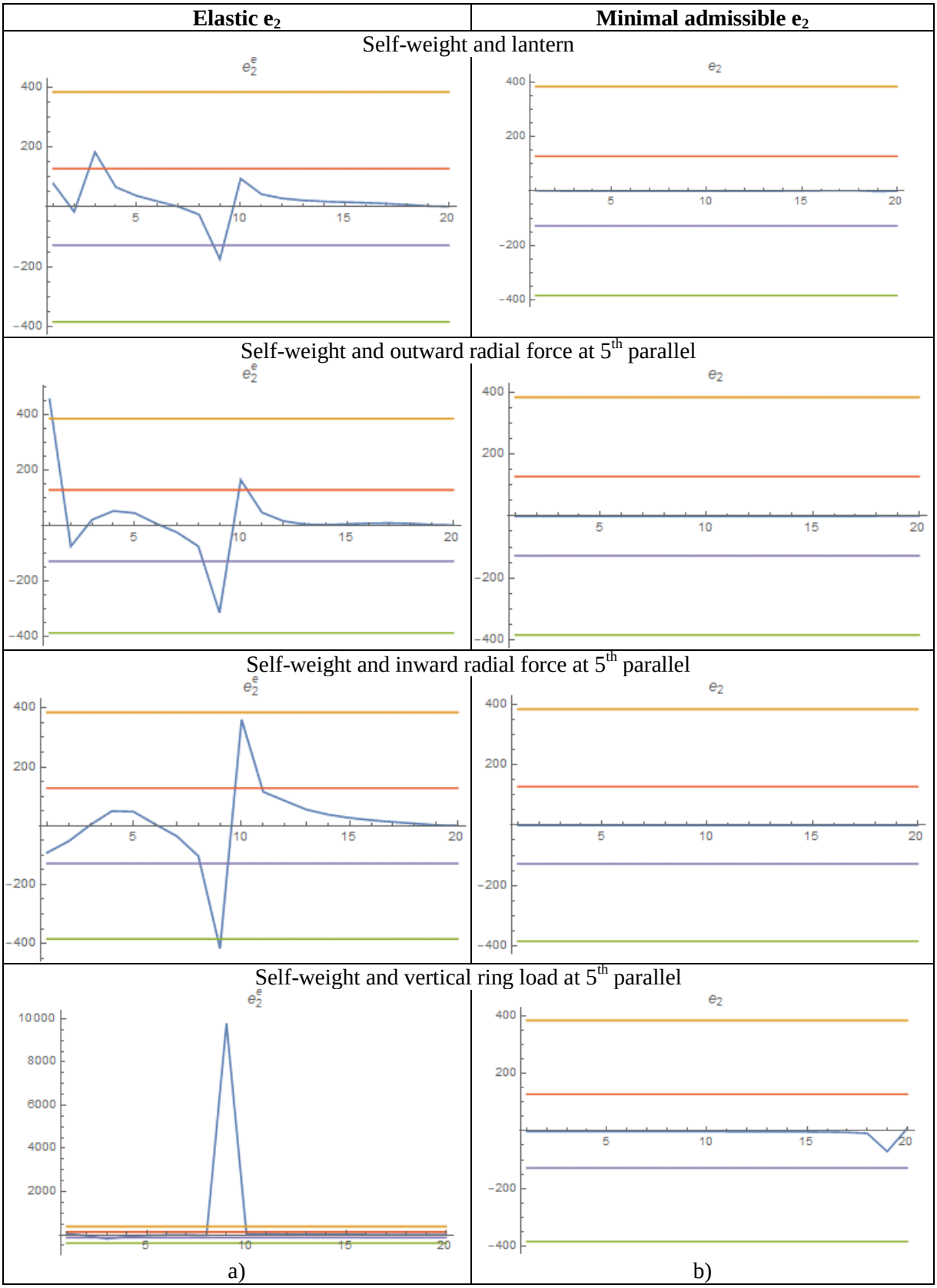

Figure 14 Trust line e_2 of the elastic solution along the meridian, solid lines represent thickness, green and orange cross-section limits lines, red and blue median third of the section

The results evidence showed that the pure elastic solution did not satisfy the compatibility requirements, and the residual resolved through the equilibrium equation in the homogenized form, did contribute to getting the eccentricity compatible with no tensile resistant material.

The second columns of Figure 9 and Figure 10 highlighted that in the analyzed cases the minimal eccentricity exists within a wide range of load multipliers that satisfies compatibility, moreover, almost totally compressed solutions represented the output of the minimization program with respect to the actual eccentricity, under prescribed large load multipliers. The results confirmed the output of the program that maximizes the load multiplier that resulted in unbounded value.

Figures 13 and 14 presented the thrust lines of several analyzed cases. It can be seen that the elastic response, often presents eccentricity outside the limits, both the central core of inertia, the middle third, or the thickness of the section. In particular, in the case of self-weight, Figure 13, and Figure 14, it let's notice that the elastic response violated the limit requirement, but the self stress was able to bring back the stress within the domain. The figure showed minimal eccentricity resulting in the optimal program that superimposed the suitable self stress able to fulfill the compatibility with the applied loads. One can recognize this behavior as typical for the domes, which, even in the presence of base swellings, or overloading, causing cracks, do not suffer global collapse since the cracks do not affect the overall stability.

The further analyzed load cases confirmed that the structure bore the loads with the contribution of self stress that are always capable in addition to the elastic response to pit the stress into the limit domain.

4. CONCLUSION

In the paper, we proposed the analysis of parabolical domes using the limit analysis. The proposed method starts with the analytical solution of spherical domes to calculate any self equilibrated stress. Moreover, a finite element elastic solution is obtained from the actual loads and was used as the purely elastic solution to be introduced into Melan's theorem. The analytical solution of the homogeneous equation of spherical domes is used to model the eigenstress of parabolical domes through an approximate interpolation of the parabola with a sphere. The approximation allowed us to use the analytical solution to a geometry inspired to Brunelleschi's Santa Maria del Fiore dome in Florence. The proposed results were presented in terms of thrust lines that are reported. The thrust lines confirmed that the parabolical domes are safe under the applied loads. The proposed method allowed us to calculate the safety factor, under prescribed load patterns, and to assess the safety of the prescribed load level. Both strategies have been presented and showed the feasibility of the method.

REFEFENCES

[1] J. Heyman, (1966) "The stone skeleton," International Journal of Solids and Structures, vol. 2, no. 2, p.

[2] D. Aita and A. Sinopoli, (2020) "Revisiting Monasterio's Unpublished Manuscript: A Critical Review of the Collapse Modes Analysis of Non-Symmetric and Symmetric Masonry Arches," International Journal of Architectural Heritage, vol. 14, no. 5, pp. 762-793.

[3] G. Cocchetti and E. Rizzi, (2020)"Analytical and numerical analysis on the collapse modes of least-thickness circular masonry arches at decreasing friction," Frattura ed Integrita Strutturale, vol. 14, no. 51, pp. 356-375.

[4] M. Pepe, M. Sangirardi, E. Reccia, M. Pingaro, P. Trovalusci and G. de Felice, (2020) "Discrete and Continuous Approaches for the Failure Analysis of Masonry Structures Subjected to Settlements," Frontiers in Built Environment, vol. 6, p.

[5] M. Gilbert, C. Casapulla and H. Ahmed, (2006) "Limit analysis of masonry block structures with non-associative frictional joints using linear programming," Computers and Structures, vol. 84, no. 13-14, pp. 873-887.

[6] V. Minutolo, S. Di Ronza, C. Eramo, P. Ferla, S. Palladino and R. Zona, (2019) "The use of destructive and non-destructive testing in concrete strength assessment for a school building," International Journal of Advanced Research in Engineering and Technology, vol. 10, no. 6, pp. 252-267.

[7] E. Bernat-Maso, L. Gil and J. Marcé-Nogué, (2012) "The structural performance of arches made of few vossoirs with dry-joints," Structural Engineering and Mechanics, vol. 44, no. 6, pp. 775-799.

[8] S. Di Ronza, C. Eramo, V. Minutolo, S. Palladino, E. Totaro, P. Ferla, R. Zona, T. Ronga and C. C. Pomicino, (2020) "Experimental tests on gully tops and manhole TOPS devices according to EN124 standard," International Journal of Advanced Research in Engineering and Technology, vol. 11, no. 2, pp. 276-295.

[9] V. Minutolo, E. Cerri, A. Coscetta, E. Damiano, M. De Cristofaro, L. Di Gennaro, L. Esposito, P. Ferla, M. Mirabile, L. Olivares and R. Zona, (2020) "NSHT: New smart hybrid transducer for structural and geotechnical applications," Applied Sciences.

[10] S. Palladino, L. Esposito, P. Ferla, E. Totaro, R. Zona and V. Minutolo, (2020) "Experimental and Numerical Evaluation of Residual Displacement and Ductility in Ratcheting and Shakedown of an Aluminum Beam," Applied Sciences, vol. 10, no. 10, p. 3610, 225

[11] J. Lubliner, (2008) Plasticity Theory, Courier Corporation, Ed.

[12] W. T. Koiter, (1960) "General theorems for elastic-plastic solids," Progress in Solid Mechanics, pp. 165-221.

[13] F. Cluni, V. Gusella and M. Schiantella, (2020) Upper bound limit analysis of quasi-periodic masonry by means of discontinuity layout optimization (Dlo), pp. 2124-2133.

[14] G. Milani, K. Beyer and A. Dazio, (2009) "Upper bound limit analysis of meso-mechanical spandrel models for the pushover analysis of 2D masonry frames," Engineering Structures, vol. 31, no. 11, pp. 2696-2710.

[15] S. W. Sloan, (1989) "Upper bound limit analysis using finite elements and linear programming," International Journal for Numerical and Analytical Methods in Geomechanics, vol. 13, no. 3, pp. 263-282.

[16] C. Baggio and P. Trovalusci, (1998) "Limit analysis for no-tension and frictional three-dimensional discrete systems," Mechanics of Structures and Machines, vol. 26, no. 3, pp. 287-304.

[17] G. Stavroulakis, I. Menemenis, M. Stavroulaki and G. Drosopoulos, (2020) Collapse prediction and safety of masonry arches, pp. 191-201.

[18] P. Lourenço, D. Oliveira, P. Roca and A. Orduña, (2005) "Dry joint stone masonry walls subjected to in-plane combined loading," Journal of Structural Engineering, vol. 131, no. 11, pp. 1665-1673.

[19] D. Oliveira, P. Lourenço and C. Lemos, (2010) "Geometric issues and ultimate load capacity of masonry arch bridges from the northwest Iberian Peninsula," Engineering Structures, vol. 32, no. 12, pp. 3955-3965.

[20] A. Mauro, G. de Felice and M. DeJong, (2015) "The relative dynamic resilience of masonry collapse mechanisms," Engineering Structures, vol. 85, pp. 182-194.

[21] F. Portioli, (2020) "Rigid block modelling of historic masonry structures using mathematical programming: a unified formulation for non-linear time history, static pushover and limit equilibrium analysis," Bulletin of Earthquake Engineering, vol. 18, no. 1, pp. 211-239.

[22] P. Block and L. Lachauer, (2014) "Three-dimensional (3D) equilibrium analysis of gothic masonry vaults," in International Journal of Architectural Heritage.

[23] A. Fraddosio, N. Lepore and M. Piccioni, (2020) "Thrust Surface Method: An innovative approach for the three-dimensional lower bound Limit Analysis of masonry vaults," Engineering Structures, vol. 202, p.

[24] N. Nodargi and P. Bisegna, (2020) "Thrust line analysis revisited and applied to optimization of masonry arches," International Journal of Mechanical Sciences, vol. 179, p.

[25] É.-H.-F. Méry, (1840) Annales des ponts et chaussées. Mémoires et documents relatifs à l'art des constructions et au service de l'ingénieur, pp. 50-70.

[26] T. V. Mele and P. Block, (2011) "A novel form finding method for fabric formwork for concrete shells," Journal of the International Association for Shell and Spatial Structures, vol. 52, no. 170, pp. 217-224, 12.

[27] F. Fraternali, "A thrust network approach to the equilibrium problem of unreinforced masonry vaults via polyhedral stress functions," Mechanics Research Communications, vol. 37, no. 2, pp. 198-204, 3 2010.

[28] A. Liew, D. Pagonakis, T. Van Mele and P. Block, (2018) "Load-path optimisation of funicular networks," Meccanica, vol. 53, no. 1-2, pp. 279-294, 1 1

[29] S. Tiberti and G. Milani, (2020) "3D homogenized limit analysis of non-periodic multi-leaf masonry walls," Computers and Structures, vol. 234, p.

[30] L. Moubax and K. De Jonge, (2018) "The dome of Saint-Paul-Saint-Louis in Paris, a historical and structural analysis," in Building Knowledge, Constructing Histories.

[31] J. Hambleton, S. Sloan, A. Pyatigorets and V. Voller, (2011) "Lower bound limit analysis using the Control Volume Finite Element Method," in Computer Methods for Geomechanics: Frontiers and New Applications.

[32] R. Seshadri and S. P. Mangalaramanan, (1997) "Lower bound limit loads using variational concepts: The mα-method," International Journal of Pressure Vessels and Piping, vol. 71, no. 2, pp. 93-106.

[33] S. Chen, Y. Liu and Z. Cen, (2008) "Lower-bound limit analysis by using the EFG method and non-linear programming," International Journal for Numerical Methods in Engineering, vol. 74, no. 3, pp. 391-415.

[34] A. Makrodimopoulos and C. M. Martin, (2006) "Lower bound limit analysis of cohesive-frictional materials using second-order cone programming," International Journal for Numerical Methods in Engineering, vol. 66, no. 4, pp. 604-634.

[35] C. V. Le, M. Gilbert and H. Askes, (2009) "Limit analysis of plates using the EFG method and second-order cone programming," International Journal for Numerical Methods in Engineering, vol. 78, no. 13, pp. 1532-1552.

[36] S. Wolfram, (1999) The Mathematica® book, 4th ed., Wolfram Media, p. 1470.